scientific reports

Check for updates

OPEN

The impact of PANoptosis-related genes on immune profiles and subtype classification in ischemic stroke

Xinrui Cai[1], Yu Ren[1], Haiyun Wu[1], Yongjun Tan[1], Li Zhou[1], Yilin Wang[1], Qinghuan Yang[1], Jiani Wang[1], Hao Tang[1], Jun Wen[1], Yong Zhao[1], Ling Wang[1], Xinlei Xu[1], Jiagui Huang[2]✉ & Qin Yang[1]✉

Ischemic stroke (IS) is an acute neurological disorder causing brain dysfunction, with high mortality and disability. PANoptosis is a synchronized sort of regulated cell demise that combines the characteristics of pyroptosis, apoptosis, and necroptosis. However, its role in ischemic stroke remains unclear. We downloaded the ischemic stroke-related microarray dataset GSE58294 from the Gene Expression Omnibus (GEO) database and identified Differentially expressed PANoptosis-related genes (DE-PRGs). We utilized three algorithms to identify diagnostic DE-PRGs, constructed a nomogram for diagnostic modeling, and evaluated their diagnostic performance with receiver operating characteristic (ROC) analysis. Additionally, we develop interaction networks linking genes with miRNAs, transcription factors, and drugs. We also analyzed gene expression in different cell subgroups using the GSE174574 single-cell dataset. We applied consensus clustering to classify stroke samples into subtypes and compared immune microenvironment differences. Ultimately, we verified the gene expression patterns of candidate markers through the MCAO model. We pinpointed seven diagnostic DE-PRGs, with CASP1, PIK3R5, AVEN, and PSMC3 showing significant protein expression differences. Single-cell transcriptome analysis revealed the link between stroke and immune cells. Furthermore, consensus clustering revealed two clusters with unique immune infiltration patterns and functional characteristics. Our study may provide new theoretical insights for the early diagnosis and targeted therapy of IS and offer support for the clinical application of PANoptosis in IS.

Keywords PANoptosis, Ischemic stroke, Immune infiltration, Immune cell, Machine learning, Molecular cluster

Abbreviations

IS	Ischemic stroke
DE-PRGs	Differentially expressed PANoptosis-related genes
SVM-RFE	Support vector machine-recursive feature elimination
AUC	Area under the curve
DEG	Differentially expressed gene
GEO	Gene Expression Omnibus
GO	Gene Ontology
GSVA	Gene set variation analysis
KEGG	Kyoto Encyclopedia of Genes and Genomes
LASSO	Least absolute shrinkage and selection operato
miRNA	MicroRNA
NK	Natural killer
PCA	Principal component analysis
PPI	Protein–protein interaction
PRGs	PANoptosis-related genes

[1]Department of Neurology, the First Affiliated Hospital of Chongqing Medical University, 1 Youyi Road, Yuzhong District, Chongqing 400016, China. [2]Department of Neurology, the Second People's Hospital of Yibin, Beida Street No 96, Yibin 644000, China. ✉email: shjwhg@126.com; xyqh200@126.com

RF	Random forest
ROC	Receiver operating characteristic
SVM	Support vector machine
TF	Transcription factor
PCD	Programmed cell death

Stroke is an acute brain injury, and ischemic stroke (IS) accounts for the majority of cases, it ranks as the world's second most common cause of mortality, accompanied by high fatality and disability rates, placing a significant strain on global health systems and society[1,2]. Ischemia promotes cell death and dysfunction through pro-inflammatory mediators, exacerbating neuroinflammation[3]. The subsequent restoration of blood flow and reoxygenation can potentially worsen brain tissue damage[4]. Current interventions, such as thrombolytic agents (e.g.tPA) and endovascular clot removal, remain limited by restricted therapeutic windows[5]. Although they aim to restore blood flow and prevent secondary damage, they fail to completely mitigate the cell damage caused by ischemia and reperfusion injury (I/R injury)[6]. Progressive neuronal degeneration and functional loss remain major challenges in treatment and rehabilitation[3]. Increasing evidence suggests that multiple forms of cell death are associated with brain ischemia-reperfusion injury, including apoptosis, necrosis, necroptosis, and PANoptosis[7]. Therefore, it is vital to investigate novel diagnostic approaches and therapeutic strategies to improve the prompt detection and management of IS. PANoptosis is one type of immune-related programmed cell demise regulated through the PANoptosome complex, which merges features of pyroptotic, apoptotic, and necroptotic pathways[8]. Lately, research has underscored the crucial function of PANoptosis in triggering and worsening brain injury following brain ischemia and cerebral I/R events, though the clear processes still require further exploration[9,10]. In addition, there is a strong connection between stroke and immune cells, and increasing evidence suggests that immune cells regulate the damage repair and inflammatory response in the central nervous system (CNS) following ischemic stroke through complex reactions, nonetheless, the core processes driving the immune response are still not well understood[3,11]. Therefore, identifying new signature genes and the role of the immune microenvironment could offer promising intervention points or pathogenic understanding for ischemic stroke.

PANoptosis, first described by Malireddi in 2019, represents a distinct inflammatory programmed cell death (PCD) pathway orchestrated by a multi-protein complex known as the PANoptosome[12]. This complex acts as a molecular scaffold, integrating key signaling components from pyroptosis, apoptosis, and necroptosis into a single, coordinated cell death cascade that cannot be fully explained by any of these pathways alone[12,13]. The assembly of the PANoptosome is critical for host defense and has been linked to cancer, infections, and autoinflammatory diseases[14,15]. Depending on the initial trigger, distinct PANoptosome complexes can form—such as the ZBP1-, AIM2-, RIPK1-, and NLRP12-PANoptosomes—each with unique sensors and regulators that dictate the specific cell death phenotype[8,16]. Recent studies have demonstrated that PANoptosis is activated during ischemia/reperfusion (I/R) injury, leading to increased expression of PANoptosome components like caspase-1/-8 and NLRP3 in retinal neurons[9,17]. While there is growing evidence that cell death in cerebral I/R injury involves a combination of apoptosis, necroptosis, and pyroptosis[7], the specific molecular mechanisms driving PANoptosis in this context remain largely unexplored. Consequently, understanding the role of PANoptosis could be vital for elucidating the progression of IS.

In this research, we carried out an intensive examination of DE-PRGs (Differentially expressed PANoptosis-related genes) and immunological traits in peripheral blood samples. In previous studies, machine learning has been increasingly utilized for medical diagnostics and mechanistic studies, including those related to ischemic stroke, due to its high predictive performance and dependability[18–20]. Therefore, we employed three machine learning (ML) algorithms to find seven key diagnostic markers that can be deployed to predict disease onset, and we enhanced diagnostic accuracy by developing a nomogram model. Additionally, we utilized stroke single-cell datasets to analyze the expression of stroke-related diagnostic biomarkers in the stroke microenvironment. Furthermore, we performed integrated clustering, assessed immune cell infiltration, and carried out pathway enrichment analysis. We also constructed regulatory networks around miRNA-gene interactions, transcriptional regulation by transcription factors, and drug-target relationships. Our study may provide new theoretical insights for the early diagnosis and targeted therapy of IS and offer support for the clinical application of PANoptosis in IS.

Methods

Experimental animals

A total of $n = 25$ C57BL/6 mice (20–25 g)were procured from the Chongqing Medical University Laboratory Animal Centre and housed in an SPF environment with a 12-hour light/dark cycle, 20 ± 3 ℃ temperature, and 55% ± 10% humidity. The mice were provided food and water suitable for survival. The number of perioperative deaths ($n = 2$), cases of intraoperative asphyxia ($n = 1$).Quality of animal care, including temperature maintenance, hydration, and postoperative monitoring, was ensured to maximize survival and minimize suffering. Approval for all methodologies was granted by the Ethics Committee of Chongqing Medical University (Approval No.: IACUC-CQMU-2023-03015), with strict adherence to ARRIVE standards.

Model of MCAO/R in mice

The MCAO (middle cerebral artery occlusion) model was induced using a procedure outlined in previous research[21]. Mice were anesthetized with isoflurane and were anesthetized with high CO_2 asphyxiation at the end of the procedure. Cessation of vital signs (absent pulse and corneal reflex) was documented, adhering to AVMA standards.

Behavioral testing

Mice from each group were randomly chosen for neurological function evaluation. To allow acclimatization, the mice were placed in the test chamber for 1 h before testing. Neurological deficits were evaluated using three scoring systems: Zea Longa (0–4)[21], Bederson (0–5)[22], and the modified Neurological Severity Score (mNSS), which are widely used to assess neurological function in animal models, where higher scores indicate more severe deficits[23]. The modified Garcia score[24], ranges from 3 (severe deficit) to 18 (no deficit).

Immunohistochemistry staining

Mouse brain samples were prepared into paraffin sections. The sections were incubated overnight at 4℃ with AVEN (1:100, R23573, Zenbio), PSMC3 (1:100, YT3884, Immunoway), and PIK3R5 (1:100, YT3708, Immunoway) antibodies. The chromogenic reaction was visualized with DAB, and the nuclei were counterstained with hematoxylin.

Cerebral infarct volume

TTC staining was used to measure infarct volume. Coronal brain sections were incubated in 2% TTC solution for 20 min at 37 °C and analyzed using ImageJ.

Quantitative Real-time PCR

We first took out the RNA and then reverse transcribed it into complementary DNA (cDNA). Subsequently, real-time PCR was performed to assess gene expression, and data was analyzed using the comparative cycle threshold method. The primer sequences are listed in Table 1.

Western blotting

Proteins were extracted from the peri-infarct region. The samples were incubated overnight at 4 °C with primary antibodies against PSMD2 (Rabbit, 1:1000, YT3888, Immunoway), PSMC3 (Rabbit, 1:1000, YT3884, Immunoway), ACIN1 (Rabbit, 1:1000, 23937-1-AP, Proteintech), BMX (Rabbit, 1:1000, YT0508, Immunoway), AVEN (Rabbit, 1:1000,R23573, Zenbio), Caspase-1/p20/p10 (Rabbit, 1:1000, 22915-1-AP, Proteintech), PIK3R5 (Rabbit, 1:1000, YT3708, Immunoway), Vinculin (Rabbit, 1:5000, 26520-1-AP, Proteintech). Afterward, the samples were incubated with horseradish peroxidase-conjugated anti-rabbit secondary antibodies (1:5000, RGAR001, Proteintech) for 1 h at room temperature (22–25 °C). Protein bands were detected with an enhanced chemiluminescence kit and analyzed using ImageJ.

Data preprocess

In this investigation, every dataset was obtained from publicly accessible repositories. Two bulk gene expression datasets were retrieved for subsequent analysis GSE58294[25] (69 Stroke, 23 Normal) and GSE16561[26](39 Stroke, 24 Normal) from GEO database (http://www.ncbi.nlm.nih.gov/geo/). GSE58294 utilized the GPL570 platform, which is the Affymetrix Human Genome U133 Plus 2.0 Array [HG-U133_Plus_2], whereas GSE16561 was based on the Illumina HumanRef-8 v3.0 expression bead chip, associated with the GPL6883 platform. All data were preprocessed and obtained by R package "GEOquery" tool[27]. The gene probes were aligned to the appropriate gene symbols. Any that lacked a valid match or corresponded to multiple symbols were removed from further consideration. The gene expression value of the duplicate gene symbol was calculated as the max value. The PANoptosis gene list consisted of the genes of pyroptosis, apoptosis, and necroptosis, and we systematically included 277 PANoptosis-related genes from previous studies[28] (Table S1). Additionally, we obtained single-cell sequencing data from GSE174574[29], which includes samples from three brains affected by stroke. The data underwent analysis in line with the recommended post-quality control measures, while cells were classified using the reference information from the original study. Detailed information for all GEO datasets used in this study is provided in Supplementary Table S8.

Differentially expressed gene (DEG) analysis and functional analysis

The R package limma[30] was utilized to detect PANoptosis-related genes (PRGs) between stroke and healthy cases in GSE58294. Notably, the threshold for significance was established at false discovery rate (FDR) < 0.05 and log2 |fold change (FC)| > 0.5. The Metascape[31] database was deployed for the subsequent Gene Ontology (GO)

Genes	Forword	Reverse
AVEN	CCAAGGAGAAACGATGATGGC	CTTAGACTGCCTCTGCCCA
ACIN1	CCTGGTTCGTCCCTTCACTT	TGGCAACGGCTTCCTCTAC
BMX	GTGGATGGAAAGTTCCTGTGTTG	ACTGCCCTTGGAATCTTCAGTAG
PIK3R5	CGACCACTCGGGCTATCAAG	CCTTCTCCAGGTTGCTCCAG
PSMC3	TTTCCAATGCCCAACGAGGA	ATGAGTGAGTTCCGTGGCTC
PSMD2	TCAGAGCCATTCCGCAGTTT	TTCAGCACATTCCCAGAGCC
CASP1	TGCTTTCTGCTCTTCAACACCA	CCAAGTCACAAGACCAGGCATAT
β-Actin	TTCAACACCCCAGCCATG	CCTCGTAGATGGGCACAGT

Table 1. The sequences of the primers for qPCR.

& Kyoto Encyclopedia of Genes and Genomes (KEGG) enrichment analyses on these PANoptosis-related DEGs, and an adjusted P value < 0.05 was considered statistically significant.

Screening and validation of PANoptosis diagnostic markers

Potentially diagnostic markers for Ischemic stroke were identified through three distinct machine-learning approaches: Random forest (RF), Least absolute shrinkage and selection operator (LASSO) regression, and the Support vector machine-recursive feature elimination (SVM-RFE). The "randomForest" R package[32] was employed to apply the random forest method in this study. This study performed LASSO logistic regression analysis utilizing the "glmnet" R package[33], and minimal lambda was deemed ideal. In our research, the optimization parameters underwent validation via 10-fold cross-validation, while the partial likelihood deviation fulfilled the predefined minimum criteria. The genes exhibiting common traits across the three previously discussed classification models were subsequently selected for further investigation. The GSE16561 dataset will be utilized as the validation set for an intensive evaluation of the relevance of diagnostic biomarkers. The predictive accuracy was evaluated using ROC curves, and the AUC scores were then determined. To assess the predictive performance of the nomogram, a calibration curve was created.

Identification of PANoptosis modification pattern

An unsupervised clustering approach was applied to 277 PANoptosis-related gene expression profiles with the "ConsensusClusterPlus" tool[34], yielding distinct groups associated with PANoptosis. The "K-Means" algorithm was utilized, using "euclidean" distance to measure similarity. Resampling involved 80% of the items, with 1000 replications performed. The best k value was determined by assessing the proportion of ambiguous clustering (PAC). Principal component analysis (PCA) was conducted to further validate the PANoptosis-related gene expression patterns in different modification patterns. Wilcox tests were conducted to compare immunocyte infiltration scores, checkpoint gene levels, and HLA expression between the two distinct modification patterns.

Biological enrichment assessment for varying PANoptosis modification patterns

GSVA was conducted to identify key pathways and core genes associated with different PANoptosis modification patterns. Additionally, enrichment analyses were undertaken to determine the biological processes that were significantly enriched. The pathways were ordered according to their normalized enrichment scores, and those with a P-value < 0.05 were chosen for subsequent analysis. To obtain the biological enrichment entries, gene ontology enrichment analysis was performed using clusterProfiler[35] R package based on differentially expressed genes (DEG) between distinct PANoptosis modification patterns.

13 Single-cell RNA-seq (scRNA-seq) data analysis

scRNA-seq data was obtained from GSE174574 and was analyzed with Seurat (https://github.com/satijalab/seurat)[36]. Cells with < 200 or > 5,000 genes and mitochondrial gene fragments > 10% were filtered. The remaining cells were merged into one gene expression count matrix, and the count data were normalized and scaled using Seurat's functions of NormalizeData() and ScaleData(). Dimension reduction and clusters identification of cells were implemented by RunUMAP () and Findclusters() functions. After cluster classification, different cell clusters were identified and annotated by SingleR[37] R package. Gene expression levels were visualized using the "featureplot" function.

CeRNA-Network construction

Transcription factors (TFs) represent a group of proteins capable of binding to particular DNA sites, thereby regulating gene expression. The interaction between common genes and transcription factors was analyzed using NetworkAnalyst 3.0[38]. MicroRNAs (miRNAs), short endogenous non-coding RNAs, are involved in the degradation of target mRNAs or the inhibition of their translation. NetworkAnalyst 3.0 served to build a shared gene–miRNA co-regulatory network based on the identified common genes. Examining protein–drug interactions helps reveal the structural details necessary for effective receptor responsiveness. The same platform was then employed to construct a shared gene–chemical drug co-regulatory network.

Statistical analysis

The statistical evaluations were conducted with R software (version 4.1.1, https://www.r-project.org/). Differences between the two groups were examined using the Wilcoxon test (mean ± SD), and a P-value below 0.05 signified statistical significance (ns: not significant; $^{*}P<0.05$, $^{**}P<0.01$, $^{***}P<0.001$, $^{****}P<0.0001$). For correlation analysis, the Pearson correlation coefficient was calculated, with P values < 0.05 considered significant. The two-tailed Student's t-test was performed using Prism 8 (GraphPad) to evaluate the differences between the two groups and analyze the experimental data.

Results

Variant landscape of PRGs in stroke patients

The flow chart illustrating the research is presented in (Fig. 1). A sum of 50 PANoptosis-related DEGs between Stroke and normal samples from the GSE58294 database were identified and displayed in (Fig. 2A,B). The expression of each of the 50 DE-PRGs in the GSE58294 is revealed in (Fig. 2C). Subsequently, we developed a protein-protein interaction diagram to reveal the complex associations among proteins linked to PANoptosis DEGs (Fig. 2D). To explore the biological functions of these 50 DE-PRGs, we performed Gene Ontology (GO) and Kyoto Encyclopedia of Genes and Genomes (KEGG) enrichment analyses. GO analysis revealed that the genes were significantly enriched in biological processes related to cell death and immune regulation, including 'intrinsic apoptotic signaling pathway', 'regulation of execution phase of apoptosis', 'positive regulation of defense

Fig. 1. A thorough flow diagram illustrating the investigation of PANoptosis-related DEGs in IS.

response', and 'regulation of response to cytokine stimulus' (Fig. 2E-F). In the KEGG pathway analysis, the DE-PRGs were primarily associated with 'Pathways of neurodegeneration-multiple diseases' and 'Pathogenic Escherichia coli infection', suggesting a link between PANoptosis, neurodegenerative processes, and host-pathogen interactions in the context of IS.

Construction of a nomogram based on PANoptosis-related genes

Stroke biomarkers possessing diagnostic value were discovered through three distinct machines. The SVM-RFE algorithm noted 44 genes (Fig. 3A, Table S2), RF model identified 12 genes (Fig. 3B, Table S3), and the Least absolute shrinkage and LASSO regression procedure singled out 18 genes (Fig. 3C-D, Table S4). A Venn diagram of these genes revealed an overlap of 7 robust core biomarkers (PSMD2, PSMC3, BMX, AVEN, PIK3R5, CASP1 and ACIN1) (Fig. 3E). Notably, this set includes CASP1, a key enzyme driving inflammatory pyroptosis and a

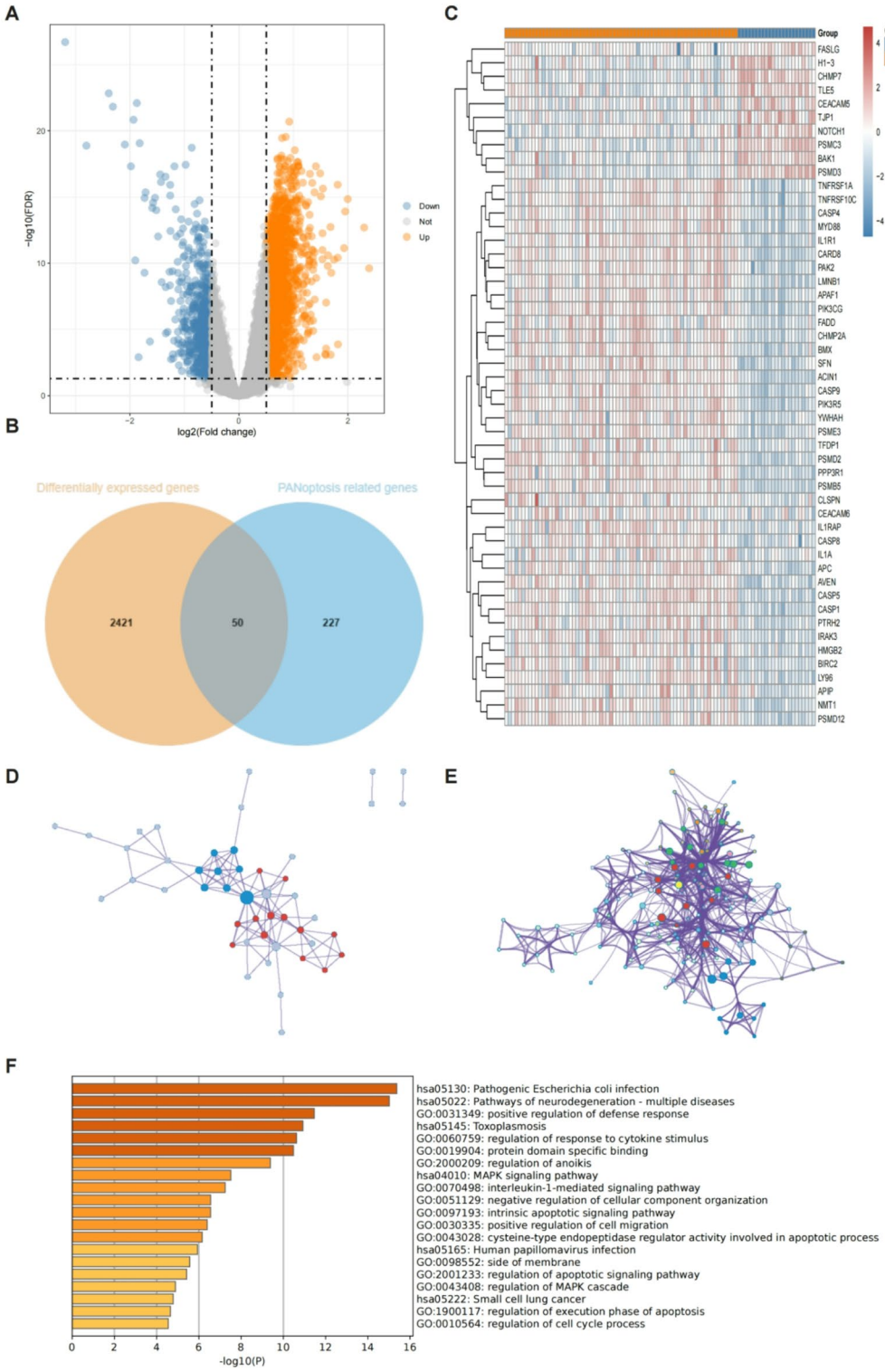

Fig. 2. Variant Landscape of PRGs in Stroke. (**A**) Volcano plot illustrating DEGs between Stroke and normal tissues (blue: down-regulated DEGs; yellow: up-regulated DEGs; grey: unchanged genes). Points with labels indicate significant Differentially expressed genes (DEGs) with FDR < 0.05 and |log2FC| > 0.5. (**B**) Venn diagram for the identification of 50 PANoptosis-related DEGs. (**C**) Heatmap of differential analysis between Stroke and normal group. Blue indicates the normal cohort, yellow denotes the stroke cohort, blue squares represent low expression, and red squares signify high expression. (**D**) Protein-protein interaction (PPI) network of PANoptosis-related DEGs. Each node represents a protein, and the edges indicate experimentally validated interactions between them. (E-F) GO term & KEGG enrichment analyses were put to use for the PANoptosis-related DEGs. The Y-axis represents enriched pathways, and the X-axis represents the gene ratio. The size of the bubble indicates the number of genes enriched in the term, and the color corresponds to the adjusted P-value.

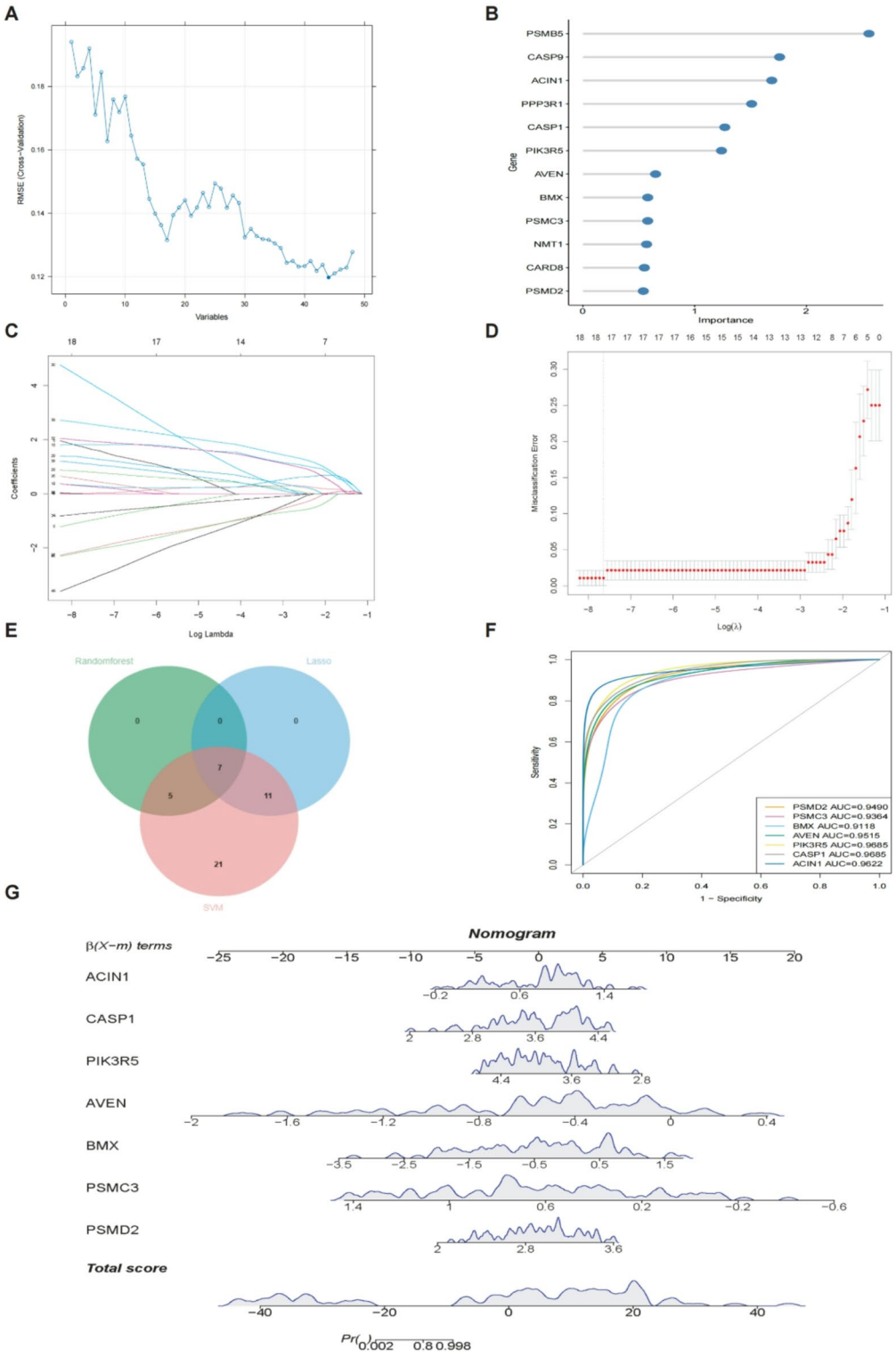

Fig. 3. Selection of Signature Genes from DE-PRGs using Machine Learning Algorithms. (**A**) Significant features selected by the SVM-RFE algorithm. (**B**) Optimal biomarkers screened by the RF algorithm. (**C**,**D**) Variable selection in the LASSO model. (**E**) Venn diagram illustrating the gene overlap among three algorithms. (**F**) ROC curves were utilized to evaluate the capability of diagnostic markers in distinguishing healthy from stroke samples, with performance quantified by the AUC value. (**G**) A nomogram was developed for Stroke prediction based on 7 genes.

known contributor to neuroinflammation following stroke. The inclusion of AVEN, an anti-apoptotic protein, and PSMC3, a proteasome subunit involved in protein homeostasis, suggests that the diagnostic signature captures a balance between pro-death and survival signals critical to neuronal fate in IS. The ROC curves indicated that every biomarker achieved an area under the curve (AUC) greater than 0.9 (Fig. 3F). The Rms package was employed to develop a stroke diagnostic nomogram (Fig. 3G). Moreover, decision curve analysis (DCA) demonstrated that this nomogram gave a higher clinical net benefit than all other strategies (Fig. 4A,B). The diagnostic line graph showed higher AUC values in both the training (GSE58294) and the validation (GSE16561) set, indicating improved model performance across both datasets (1.000, 0.949, respectively; Fig. 4C,D). Stroke samples exhibited a markedly higher Hypoxia risk score compared to healthy samples (Fig. 4E,F). These findings reinforce the enhanced predictive accuracy of the diagnostic nomogram.

Identification and interaction network analysis of candidate diagnostic biomarkers

To uncover the regulatory mechanisms of candidate diagnostic genes was constructed. Furthermore, miRNAs with cross-linking were picked to certify the accuracy and reliability of the results. 383 miRNAs and 7 potential biomarkers regulatory networks were obtained (Fig. 5A, Table S5). Notably, hsa-mir-103a-3p, hsa-let-7a-5p, hsa-let-7c-5p, and hsa-let-7f-5p appear to potentially regulate most of the candidate diagnostic genes concurrently. Ultimately, our results revealed 34 transcription factors that affect candidate diagnostic genes (Fig. 5B, Table S6). Additionally, CREB1 may simultaneously regulate PIK3R5, CASP1, BMX, and PSMC3, whereas FOXC1 could concurrently influence BMX, PIK3R5, PSMC3, and ACIN1. Drug–gene interaction data from the NetworkAnalyst database identified 160 potential target drugs/compounds, and a network was constructed using seven candidate biomarkers (Fig. 5C, Table S7). There were interactions between drugs/compounds and most of the potential biomarkers, such as interactions between cobaltous chloride, Cyclosporine, Tetrachlorodibenzodioxin, Valproic Acid, and most of the potential biomarkers. These promising drugs or chemical compounds may exert a therapeutic effect on recurrent procedures by targeting diagnostic biomarkers.

Single-cell transcriptome data analysis

Using the GSE174574 single-cell dataset, we evaluated the level of expression for diagnostic biomarkers associated with stroke within its microenvironment. After integrating data from three stroke samples in the GSE174574 dataset, we identified 31,212 cells. We then removed cells that had fewer than 200 or more than 5,000 total RNAs, as well as those with a mitochondrial UMI rate exceeding 10%. After identifying the top 2000 highly variable genes, we applied a linear dimensionality reduction technique to characterize the intrinsic structure of the dataset. The initial 15 principal components were subsequently utilized to generate a UMAP visualization that effectively captures the primary variance within the data. The Stroke dataset comprises 19 distinct cell populations and 9 primary cell types (Fig. 6A,B), including Endothelial, Epithelial, Fibroblast, Granulocyte, Macrophage, Microglia, Monocyte, NK and Oligodendrocyte cells. The majority of these were Endothelial, Macrophage, and Microglia cells. PSMD2 is primarily exhibited in Oligodendrocyte and Macrophage cells; PSMC3 is chiefly exhibited in Fibroblast, Endothelial, and Macrophage; CASP1 is mainly exhibited in Monocyte; ACIN1 is mainly expressed in NK cells (Fig. 6C). Diagnostic biomarkers expressed in various cells are shown in the (Fig. 6D).

3.5 Identifying diagnostic biomarkers related to molecular subgroups and differences in the immune microenvironment between subgroups in Stroke.

To explore the association between the levels of expression of 277 PANoptosis-related genes and stroke subtypes, we conducted a consensus clustering analysis on all 69 IS patients from the GSE58294 dataset. By testing cluster numbers from 2 to 10, we determined that $k = 2$ yielded the highest intra-cluster similarity (Fig. S2) and the lowest inter-cluster similarity, suggesting that these genes effectively classify stroke patients into two distinct groups (Fig. 7A). Cluster A comprised 38 cases, while Cluster B consisted of 31 cases. As shown in (Fig. 7B), the amount of expression in HLA-A, HLA-B, HLA-C, HLA-E, HLA-F, and HLA-G were significantly higher in ClusterB than in patients in Cluster A, while HLA-DOA and HLA-DOB were significantly higher in ClusterA than in patients in ClusterB. In terms of immune checkpoints, the expression of BTLA, CD28, CD200R1, CTLA4, ICOS, and TIGIT was notably higher in the Cluster A group compared to Cluster B. Conversely, the levels of LGALS9, TNFRSF8, TNFRSF9, and TNFSF14 were markedly lower in Cluster A (Fig. 7C). Cluster A was characterized by a higher infiltration of M2 macrophages and regulatory T cells (Tregs). In the context of ischemic stroke, this immune profile may represent a less inflammatory or pro-reparative endotype, as M2 macrophages and Tregs are known to suppress inflammation and promote tissue repair, potentially leading to better clinical outcomes. (Fig. 7D).

To explore the underlying molecular mechanism between PANoptosis-related subtypes, we screened out a total of 426 subtype-related genes. The PPI network was constructed using the Metascape database and The MCODE plug-in analyzes the critical modules of the PPI network diagram, and 6 modules were identified (Fig. 7E). The evidence from GO/KEGG analysis indicated that DEGs between the ClusterB and ClusterA were closely involved in chromosome separation, DNA metabolic process, ATP-dependent activity, B cell activation, Allograft rejection, and Intestinal immune network for IgA production (Fig. 7F,G). Gene Set Variation Analysis (GSVA) shows that Cluster A was mainly associated with mRNA modification, mRNA methylation, mitotic DNA replication checkpoint signaling, mismatched DNA binding, mismatch repair complex binding, while Cluster B was mainly associated with proteasome core complex, beta-subunit complex, Toll-like receptor binding, superoxide-generating NAD(P)H oxidase activity, negative regulation of NK cell activation and neutrophil activation involved in immune response (Fig. 7H).

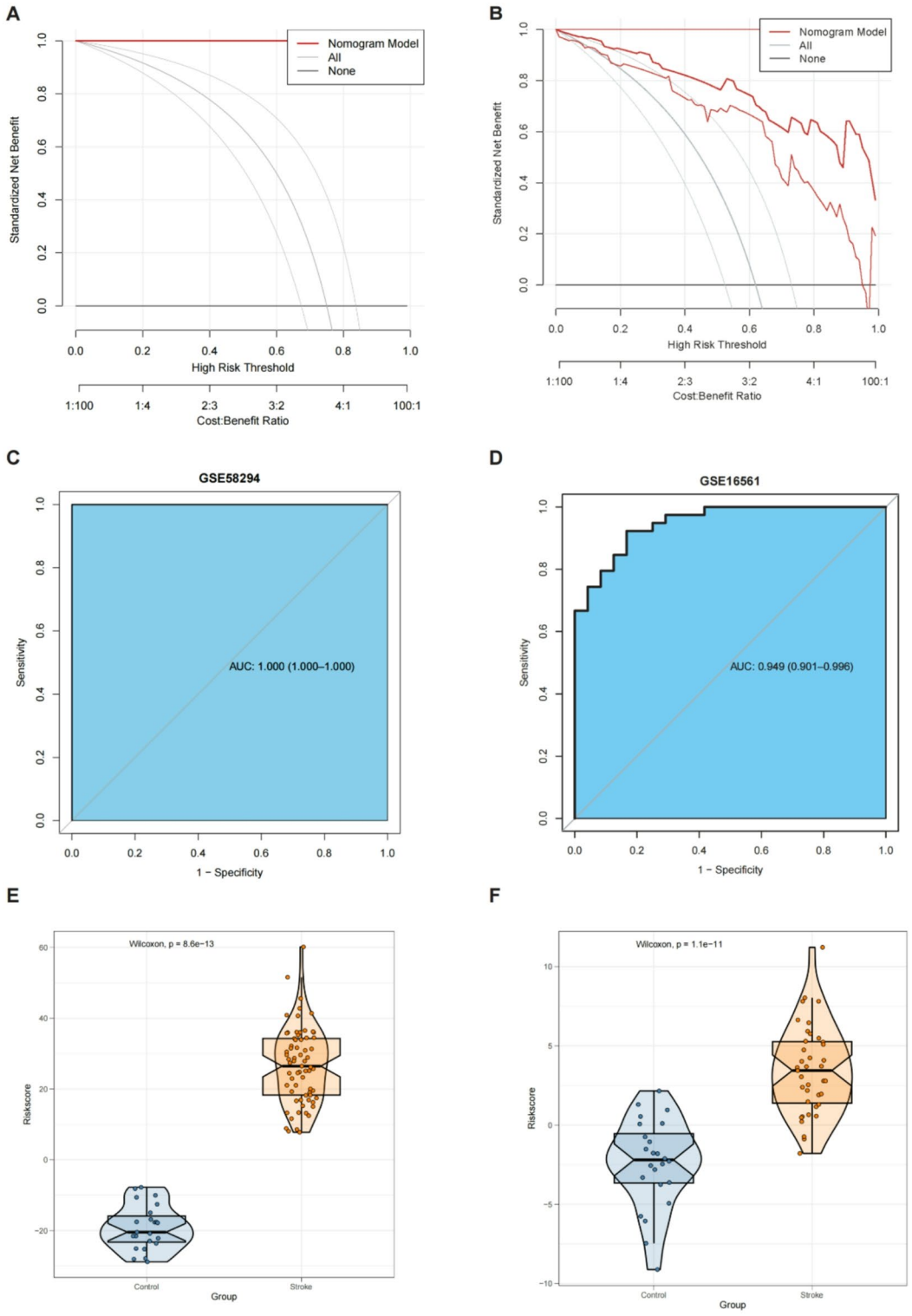

Fig. 4. Validation analysis of nomogram model in Stroke. (**A**,**B**) DCA was performed to evaluate the risk prediction nomogram for IS in the GSE58294 and GSE16561 datasets. (**C**,**D**) ROC curve analysis was conducted to validate the risk prediction nomogram for IS using data from GSE58294 and GSE16561. (**E**,**F**) Risk distribution analysis showed that IS samples consistently exhibited significantly higher risk scores than healthy samples in both GSE58294 and GSE16561.

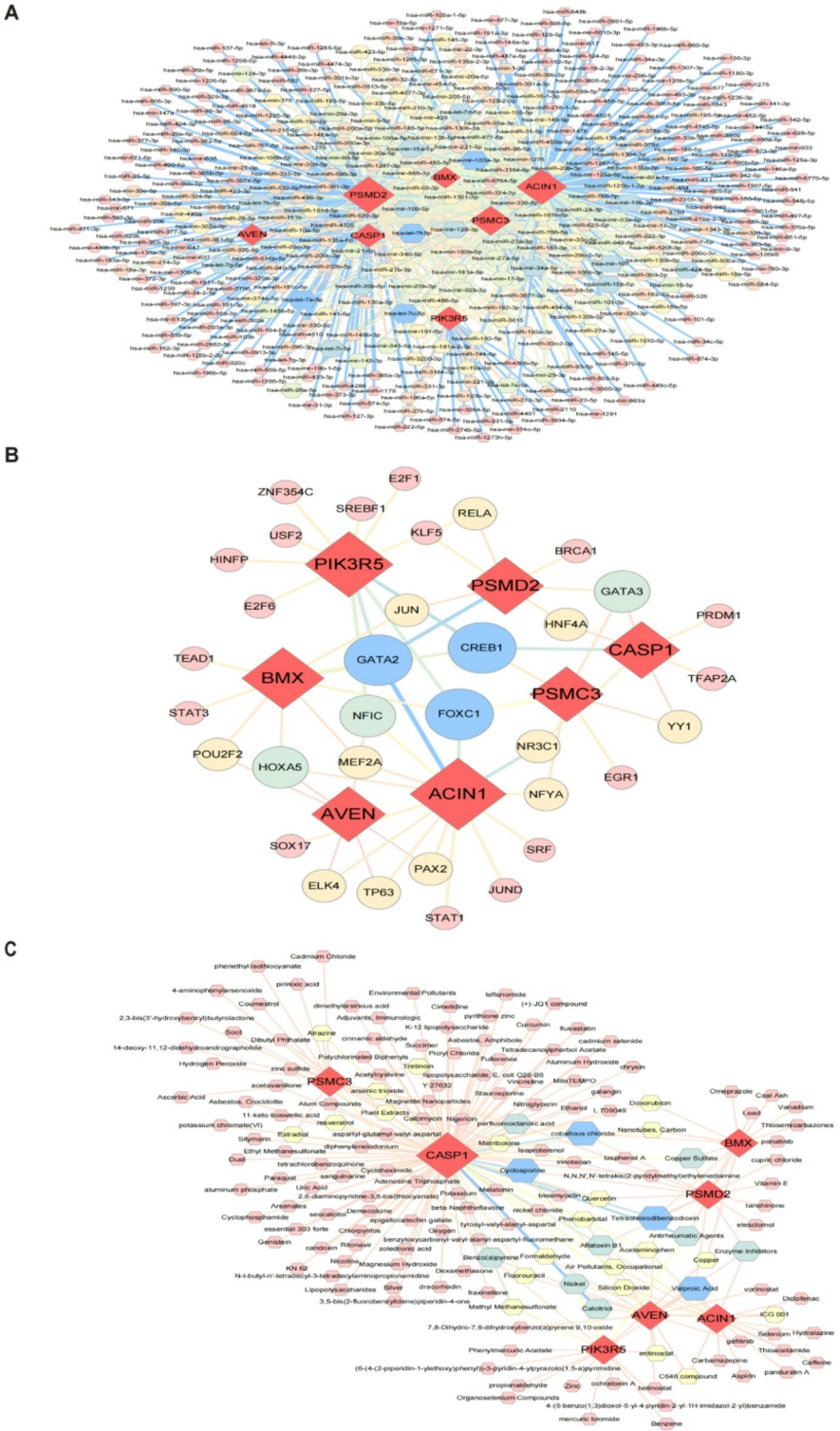

Fig. 5. The regulatory networks of diagnostic markers in Stroke. (**A**) The regulatory network involves 383 miRNAs and 7 diagnostic markers. (**B**) The regulatory network consists of 34 TFs and 7 diagnostic markers. (**C**) The drug-gene interaction network involves 160 prospective candidate drugs/compounds and 7 diagnostic markers.

The expression level of PANoptosis-Related genes in MCAO mice

To further validate the diagnostic role of these biomarkers, we first constructed an MCAO-induced IS mouse model. Twenty-four hours after reperfusion, we assessed the neurological function of the mice, as shown in (Fig. 8A). Behavioral tests indicated that, based on Zea Longa, Bederson, mNSS, and modified Garcia scores,

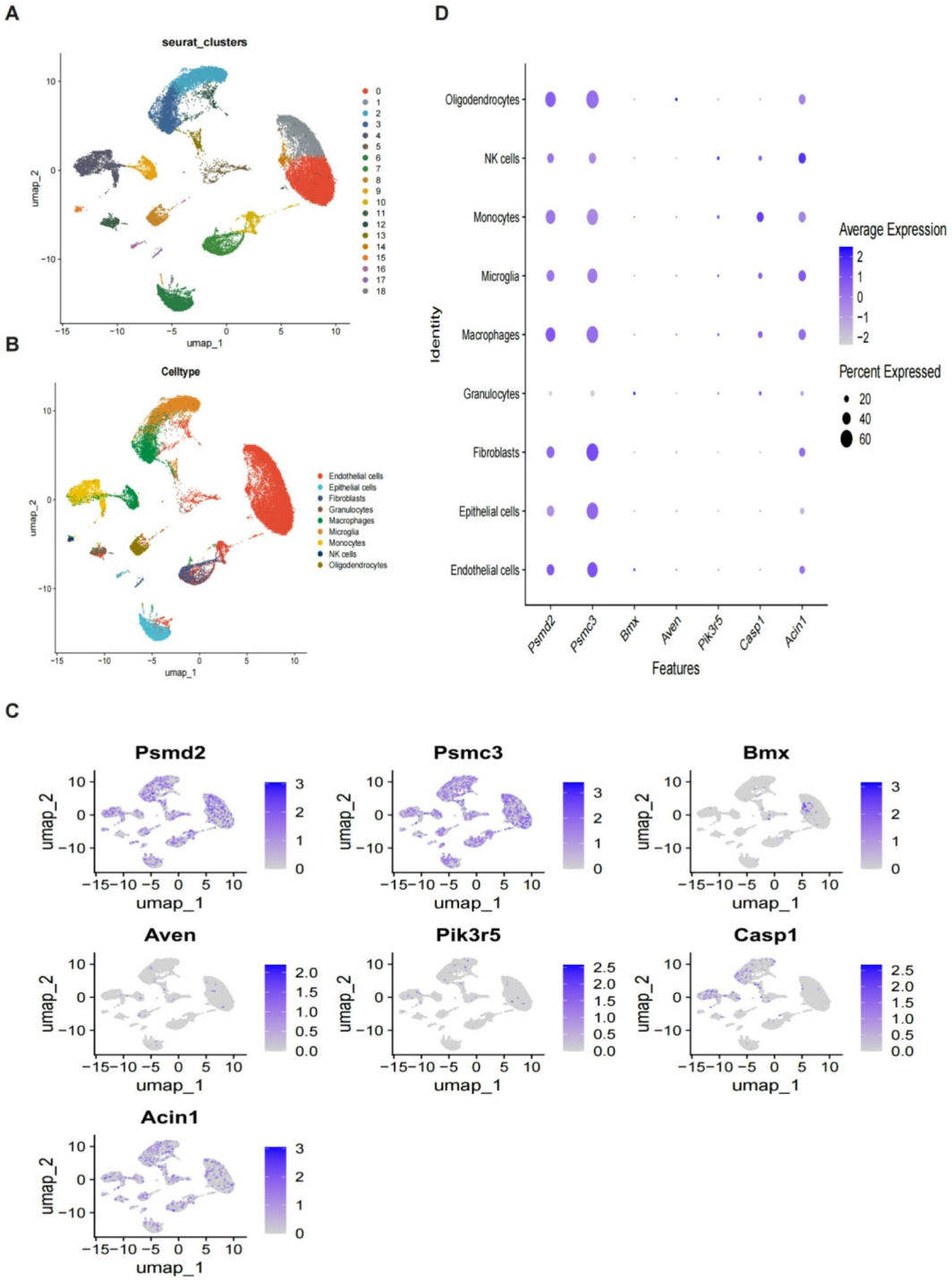

Fig. 6. Stroke-related diagnostic biomarkers in the single-cell transcriptome. (**A**) A UMAP plot representing the 19 clusters across 31,212 cells from three IS samples. (**B**) Cell types identified by marker genes. (**C**) The feature plot of the diagnostic biomarkers in different cell types. (D) Bubble plot of the average and percent expression of diagnostic biomarkers.

the MCAO group showed significant deterioration in neurological function compared to the sham group. We determined the infarct area by staining brain sections with TTC, as shown in (Fig. 8B). The qPCR results from cortical tissue were consistent with previous findings (Fig. 8C). Western blot analysis of brain tissue showed that, compared to the Sham group, the levels of PIK3R5, AVEN, and Cleaved Caspase-1 were notably elevated in the MCAO mice, while the expression of PSMC3 was significantly lower (Fig. 8D-E). Immunohistochemistry staining revealed that PIK3R5 and AVEN expression levels were notably increased in MCAO mice, whereas

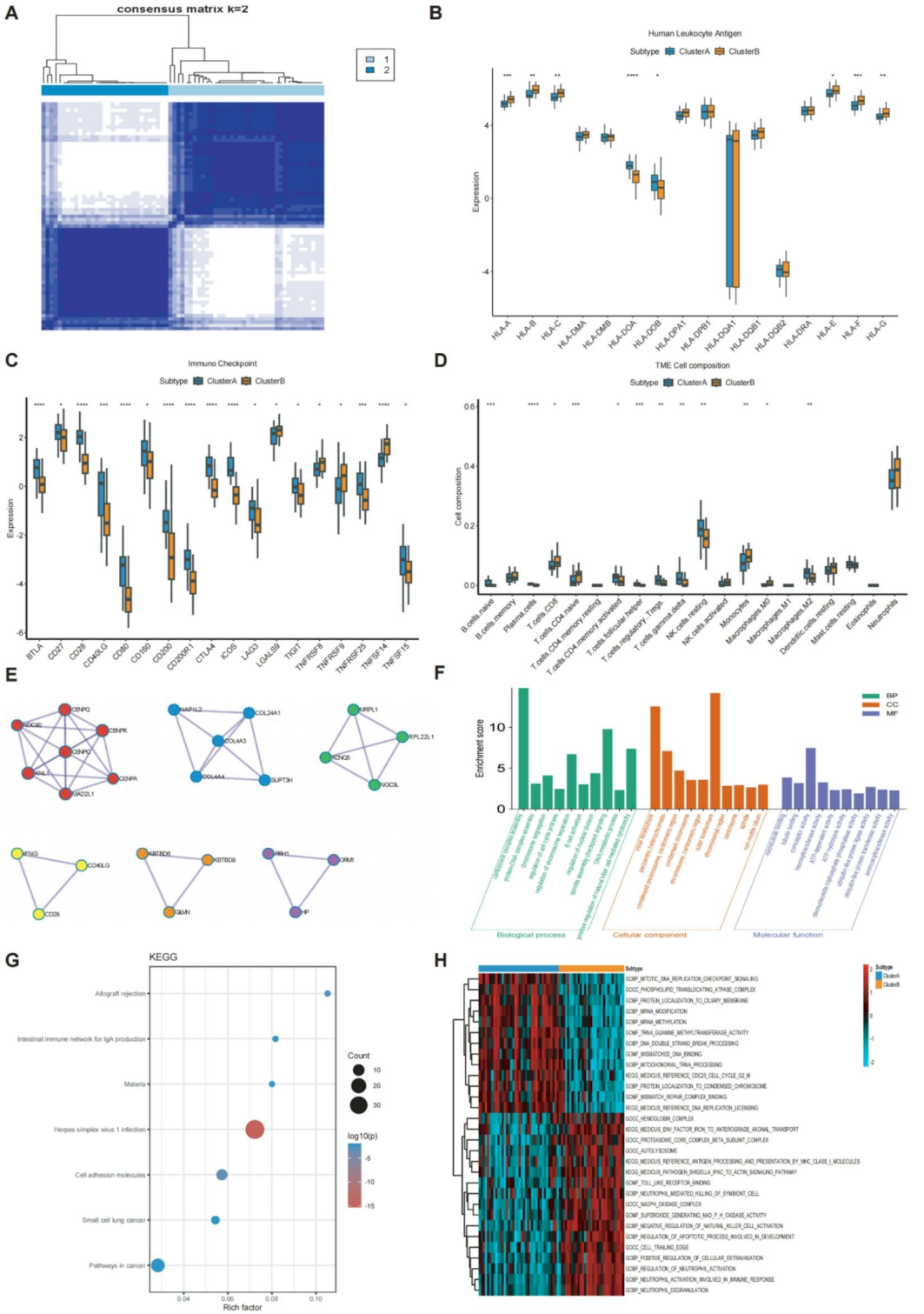

Fig. 7. Unsupervised clustering of IS-related diagnostic biomarkers. (**A**) Two clusters had the best cluster distinction. (**B**) The expression variations of each HLA gene across the two PANoptosis-related patterns. (**C**) The activity variations of each immune checkpoint gene across the two PANoptosis-related patterns. (**D**) The variations in the abundance of each immune microenvironment-infiltrating immunocyte across the two PANoptosis-related patterns. (**E**) The MCODE subnetworks are identified by the Molecular Complex Detection (MCODE) algorithm. (**F**) GO bar plot of enriched GO terms of DEGs between PANoptosis-related patterns. (**G**) KEGG bar plot of enriched KEGG pathways of DEGs between PANoptosis-related patterns. (**H**) GSVA functional enrichment analysis between PANoptosis-related patterns.

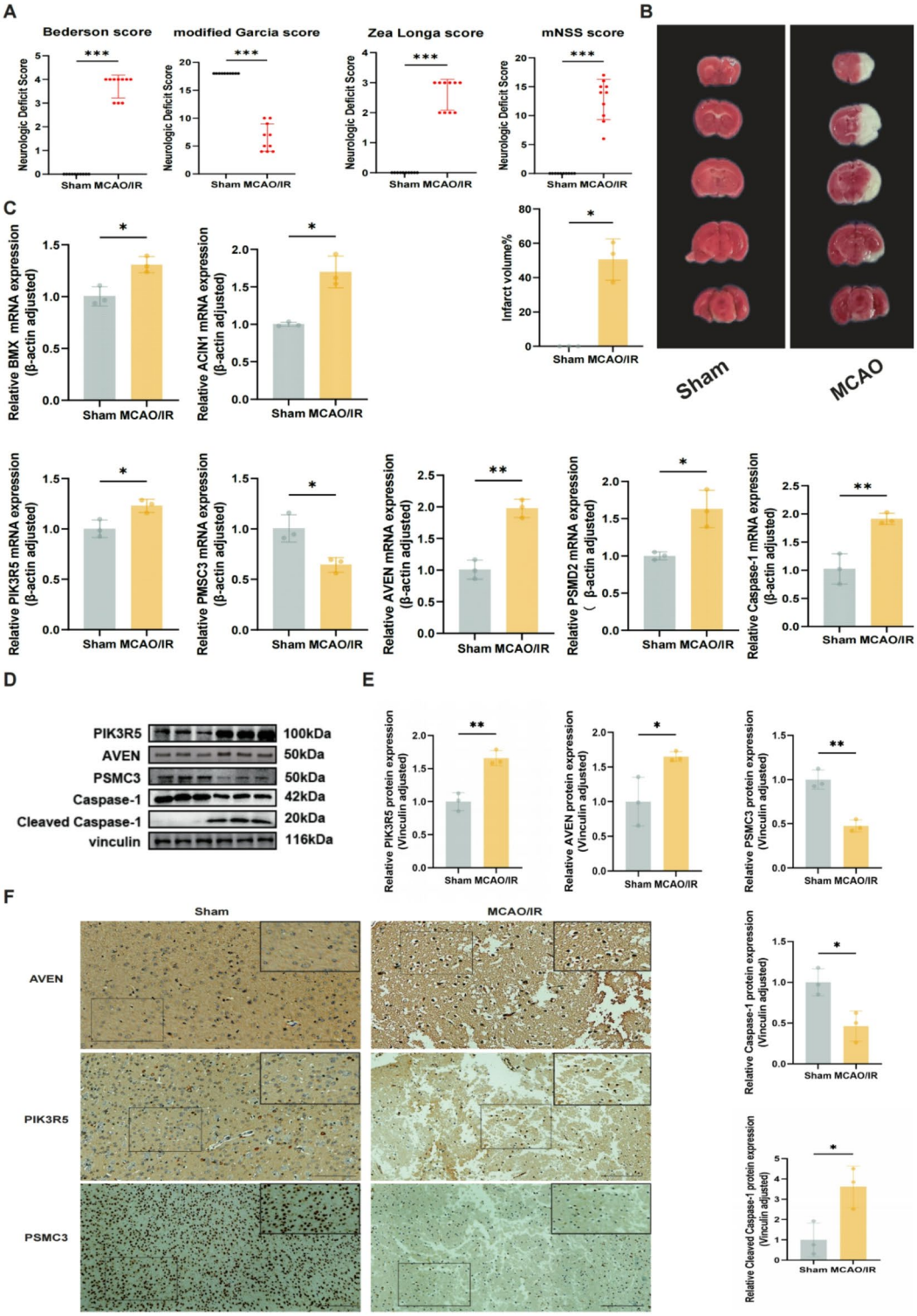

Fig. 8. In vivo validation of IS-related diagnostic biomarkers. (**A**) Neurological deficit score in different scales (**B**) TTC staining showing differences in infarct area between the two groups in the cortical region. (**C**) qRT-PCR results show that the abundance of BMX ($P = 0.0117$), ACIN1($P = 0.0268$), PIK3R5 ($P = 0.0255$), PSMC3 ($P = 0.0147$), AVEN($P = 0.0013$), PSMD2 ($P = 0.0133$) and CASP1 ($P = 0.0059$) in Sham and MCAO. (**D**) Western blotting of PIK3R5, AVEN, PSMC3, Cleaved Caspase-1, and Vinculin after MCAO. (**E**) Analysis of PSMC3 ($P = 0.0020$), AVEN($P = 0.0346$), Caspase-1($P = 0.0200$), Cleaved Caspase-1 ($P = 0.0260$) and PIK3R5 ($P = 0.0030$) after MCAO. (**F**) The representative images of immunohistochemistry analysis for AVEN, PSMC3, and PIK3R5 in brain tissue. Scale bars: 100 μm.

PSMC3 expression levels were significantly reduced (Fig. 8F). Therefore, these four genes may represent potential candidates associated with PANoptosis-related processes in ischemic stroke.

Discussion

In this research, we explored the candidate biomarkers of PRGs in IS by utilizing bioinformatics analysis and machine learning We identified seven signature genes: PSMD2, PSMC3, BMX, AVEN, PIK3R5, CASP1, and ACIN1. Among them, CASP1, PIK3R5, AVEN, and PSMC3 showed notable differences in protein expression between the MCAO and Sham group. In the ScRNA-seq profile, we found that endothelial cells, macrophages, and microglial cells represented the largest proportions, indicating a close relationship between stroke and immune cells. Furthermore, through consensus clustering, we divided IS patients into two subtypes and observed significant differences in the immune microenvironment between these subtypes.

First, we conducted the first comprehensive analysis of the distinct gene expression profiles of PRGs by comparing normal samples with those from IS. Our analysis uncovered 50 PRGs in IS patients, suggesting that PANoptosis could be a crucial element in the development of the condition. Additionally, enrichment analysis indicated that these PRGs are mainly associated with Pathogenic Escherichia coli infection, Pathways of neurodegeneration-multiple diseases, positive regulation of defense response, regulation of response to cytokine stimulus, regulation of anoikis, intrinsic apoptotic signaling pathway, regulation of execution phase of apoptosis and regulation of cell cycle process.

Recently, machine learning has been extensively applied in the diagnosis of IS, pinpointing critical genes, and the study of immune cell-associated mechanisms due to its excellent predictive performance, low error rate, and good stability[19,20]. In our study, we selected seven feature genes—PSMD2, PSMC3, BMX, AVEN, PIK3R5, CASP1, and ACIN1—using three algorithms. These seven signature genes demonstrated accurate assessment metrics across both the training and validation cohorts, the AUC values were greater than 0.9. Additionally, the nomogram containing these seven genes can combine the features to better diagnose the occurrence of IS.

CASP1, as a key component of the inflammasome, was identified as one of the important feature genes in our machine learning screening. Research has demonstrated that Caspase-1 is crucial for ischemic stroke, primarily through mediating pyroptosis, disrupting the blood-brain barrier (BBB), and triggering excessive inflammatory responses[39]. Inhibiting Caspase-1 and its associated signaling pathways, such as the NLRP3/ASC/Caspase-1 pathway, can effectively alleviate brain edema, neural damage, and secondary injury[40]. Our experimental results indicate that, in ischemic stroke (IS) samples, CASP1 mRNA expression was significantly elevated, and the activated form of Caspase-1 (such as the p20 protein) was also significantly increased in stroke patient samples, indicating that its transcriptional and translational processes might be activated synergistically. This indicates that Caspase-1 activation is closely related to inflammasome-mediated cell death (such as pyroptosis, apoptosis, and necroptosis), which is consistent with previous reports[41,42]. Additionally, we investigated the roles of other associated genes. For instance, PSMC3 is a core subunit of the 26 S proteasome, a critical complex for cellular protein degradation. Mechanistically, ischemic injury leads to an accumulation of misfolded and damaged proteins, which can trigger cellular stress and apoptosis. A downregulation of PSMC3, as observed in our study, would impair proteasomal function, exacerbate this proteotoxicity, and contribute to neuronal death. Furthermore, impaired proteostasis is known to trigger sterile inflammation, thereby linking PSMC3 dysfunction directly to the immune modulation observed in stroke[43]. PSMD2 is prominently found in various cancers and is strongly linked to poor cancer prognosis and immune evasion[44–46]. Most literature indicates that Bmx/Etk regulates cell apoptosis and cancer cell growth, with its cell-specific functions identified in various types of cancer cells[47]. Furthermore, in ischemic brain injury, Bmx/Etk regulates inflammation cell recruitment, chronic inflammation, and angiogenesis, and affects IL-6 production induced by Toll-like receptor activation[48]. AVEN functions as a crucial anti-apoptotic protein by binding to APAF-1 and inhibiting the formation of the apoptosome, a key step in the intrinsic apoptotic pathway. In the context of ischemic stroke, where neurons are under immense metabolic stress, an upregulation of AVEN could represent a compensatory, neuroprotective response aimed at counteracting pro-death signals. Its identification as a diagnostic marker suggests that the dynamic balance between pro- and anti-apoptotic factors is a central feature of the acute phase of stroke, and its modulation could be a therapeutic target[49]. The activation of PIK3R5 has an impact on acute leukemia by engaging in the activation of PI3Kγ[50]. ACIN1 could be a crucial element in the apoptosis mechanism of cells and is sometimes involved in post-transcriptional regulation[51]. It is noteworthy that PSMC3, PSMD2, PIK3R5, AVEN, and ACIN1 have not been reported in the context of IS before, making it necessary to further investigate their exact biological roles in the disease. We also validated the mRNA levels of these genes in mouse brain tissue, which were consistent with our screening results, indicating that the screening results are reliable. Interestingly, the protein expression differences of some feature genes in brain tissue were not significant. While transcriptomics provides important perspectives, it should be emphasized that gene function relies on the proteins they encode, and it cannot capture key processes like post-transcriptional and post-translational regulation, which are vital for proper protein function[52,53]. Therefore, the specific mechanisms still require further investigation.

Furthermore, we analyzed the correlations of these feature genes, including miRNA, TF, and drug-regulated interaction networks, which may offer guidance on subsequent IS-targeted and immune therapies. Many studies have demonstrated that hsa-miR-103a-3p promotes apoptosis of colorectal cancer cells by inhibiting the TGF-β pathway[54], while hsa-let-7a-5p regulates immune genes and cell death in allergic diseases and Parkinson's disease[55,56]. hsa-let-7c-5p promotes viral replication and cell apoptosis by inhibiting MAP4K4[57], and hsa-let-7f-5p affects cell death in mood disorders by regulating gene stability and immune responses[58]. These miRNAs are closely related to cell death. However, how these miRNAs simultaneously regulate most of the candidate diagnostic genes and the mechanisms of IS still require further experimental validation. In addition, many studies have shown that CREB1 and Foxc1 are important transcription factors and play roles in IS. The former plays a key role in neuroprotection, particularly under ischemic injury and excitotoxic stimuli, by responding

to extracellular signals such as growth factors and ischemic stress, activating genes containing the CRE motif[59]. CREB promotes the expression of BCL-2 through phosphorylation, exerting anti-apoptotic effects, reducing neuronal death, and potentially contributing to ischemic tolerance[60–62]. The latter, Foxc1, has a transcriptional repressive domain and is involved in regulating oxidative stress, apoptosis, and inflammation in pathological processes. Overexpression of Foxc1 can alleviate inflammatory responses and significantly reduce brain injury in a mouse model of cerebral ischemia[63]. Therefore, the important potential regulatory roles of CREB1 and Foxc1 on feature genes warrant further exploration. In the future, we plan to further investigate their underlying mechanisms in IS through molecular biology experiments.

Meanwhile, in the Single-cell transcriptome data analysis, we revealed the expression patterns of different cell populations and feature genes in IS. We found that endothelial cells, macrophages, and microglial cells represented the largest proportions. Some feature genes were notably expressed in immune cells; for example, PSMC3 was chiefly localized in fibroblasts, endothelial cells, and macrophages, while CASP1 was mainly localized in monocytes. ACIN1 was predominantly localized in NK cells. However, the function of immune cells in stroke is complex and varied. For instance, microglial cells can exert both neurotoxic and protective effects during ischemic stroke, as they are the major resident macrophage population in the brain[3]. In the ischemic brain, neutrophils constitute one of the earliest immune cell groups to arrive; they trigger tissue injury by discharging elastase, matrix metalloproteinase − 9, and ROS, each of which exacerbates the damage[64,65]. Mast cells are a contributing element in stroke by modulating vascular permeability and releasing vasoactive molecules upon degranulation, which leads to brain edema, blood-brain barrier disruption, and neutrophil infiltration[66]. Monocytes intensify the pathological cascade of IS by secreting pro-inflammatory cytokines and upregulating CB2 receptor expression, which collectively compromise the blood-brain barrier[67,68]. NK cells also play a significant role in ischemic brain injury[69]. Furthermore, different T cell subsets have distinct roles in stroke. Pro-inflammatory T cell subsets, such as CD4 + Th1, Th17 cells, γδ T cells, and CD8 + T cells, worsen stroke damage and pathology[70,71]. In contrast, Treg cells have a protective effect[72]. Their presence is key in actively suppressing autoimmune responses and maintaining immune homeostasis, thus limiting inflammatory damage[73]. Treg cells improve stroke outcomes by promoting tolerance to brain antigens and secreting IL-10[74]. In comparison, M2 macrophages exert anti-inflammatory effects through polarization by cytokines, and they could be a key element in clearing debris, stimulating tissue repair, and angiogenesis, and inhibiting inflammation[75]. Our clustering analysis identified two distinct groups among IS patients. Group A patients exhibited higher levels of Treg cells and M2 macrophage proportions. Additionally, GSVA showed that Group B was associated with superoxide generation through NAD(P)H oxidase activity and neutrophil activation involved in immune responses. Thus, Group A patients may have better prognoses. Targeted therapy focused on different immune cells may become an important direction for future stroke treatment strategies. These results partially unveil the levels of feature genes across different cell types, but the specific mechanisms of PANoptosis-related genes in immune cells during the stroke pathological process still require further exploration.

It is crucial to recognize that this study has several limitations. First, our experimental validation was conducted exclusively in an in vivo MCAO model. While this provides strong evidence, future in vitro studies using models like oxygen-glucose deprivation (OGD) on specific cell types (e.g., neurons, astrocytes) would be valuable for dissecting the precise molecular mechanisms of these key genes. Second, our diagnostic nomogram was validated bioinformatically on an independent dataset but has not yet been tested on external clinical samples. Prospective studies with patient cohorts are essential to confirm its clinical utility and predictive accuracy. Third, the sample sizes in the public datasets, while adequate for this discovery-phase study, are moderate. Validation in larger, multi-center cohorts is needed. Furthermore, our experimental validation in the MCAO model focused on the peri-infarct cortex as a whole. Future studies employing techniques like laser-capture microdissection to separately analyze the ischemic core, penumbra, and more distant regions would provide a more granular understanding of the spatial dynamics of these PANoptosis-related genes, including potential neuroprotective responses in specific brain structures. Finally, our analysis could not incorporate detailed clinical features such as stroke subtype or long-term outcomes, which should be a focus of future clinical research.

Data availability

The datasets supporting the conclusions of this article are available in the [Gene Expression Omnibus database] repository, [https://www.ncbi.nlm.nih.gov/geo/]. The GEO accessions are [GSE58294], [GSE16561], [GSE174574].

Received: 29 May 2025; Accepted: 18 September 2025
Published online: 24 October 2025

References

1. Collaborators, G. Global, regional, and national burden of stroke, 1990–2016: A systematic analysis for the global burden of disease study 2016. *Lancet Neurol.* **18**, 439 (2019).
2. Campbell, B. C. V. et al. Ischaemic stroke. *Nat. Rev. Dis. Primer.* **5**, 1–22 (2019).
3. Xu, S., Lu, J., Shao, A., Zhang, J. H. & Zhang, J. Glial cells: role of the immune response in ischemic stroke. *Front. Immunol.* **11**, 294 (2020).
4. Datta, A. et al. Cell death pathways in ischemic stroke and targeted pharmacotherapy. *Transl Stroke Res.* **11**, 1185–1202 (2020).
5. Liu, S., Luo, W. & Wang, Y. Emerging role of PARP-1 and parthanatos in ischemic stroke. *J. Neurochem.* **160**, 74 (2021).
6. Kalogeris, T., Baines, C. P., Krenz, M. & Korthuis, R. J. Cell biology of ischemia/reperfusion injury. *Int. Rev. Cell. Mol. Biol.* **298**, 229 (2012).
7. Jurcau, A. & Simion, A. Neuroinflammation in cerebral ischemia and ischemia/reperfusion injuries: from pathophysiology to therapeutic strategies. *Int. J. Mol. Sci.* **23**, 14 (2022).
8. Sun, X. et al. PANoptosis: mechanisms, biology, and role in disease. *Immunol. Rev.* **321**, 246–262 (2024).

9. Sun, Y. & Zhu, C. Potential role of PANoptosis in neuronal cell death: commentary on PANoptosis-like cell death in ischemia/reperfusion injury of retinal neurons. *Neural Regen Res.* **18**, 339 (2023).
10. Yan, W. T. et al. Do pyroptosis, apoptosis, and necroptosis (PANoptosis) exist in cerebral ischemia? Evidence from cell and rodent studies. *Neural Regen Res.* **17**, 1761 (2022).
11. Iadecola, C., Buckwalter, M. S. & Anrather, J. Immune responses to stroke: mechanisms, modulation, and therapeutic potential. *J. Clin. Invest.* **130**, 2777–2788 (2020).
12. Malireddi, R. K. S., Kesavardhana, S. & Kanneganti, T. D. ZBP1 and TAK1: master regulators of NLRP3 inflammasome/pyroptosis, apoptosis, and necroptosis (PAN-optosis). *Front Cell. Infect. Microbiol* **9** (2019).
13. Sundaram, B. et al. NLRP12-PANoptosome activates PANoptosis and pathology in response to Heme and pamps. *Cell* **186**, 2783–2801e20 (2023).
14. Chen, W., Gullett, J. M., Tweedell, R. E. & Kanneganti, T. D. Innate immune inflammatory cell death: PANoptosis and PANoptosomes in host defense and disease. *Eur. J. Immunol.* **53**, e2250235 (2023).
15. Hu, X. et al. PANoptosis signaling enables broad immune response in psoriasis: from pathogenesis to new therapeutic strategies. *Comput. Struct. Biotechnol. J.* **23**, 64–76 (2023).
16. Zheng, M., Karki, R., Vogel, P. & Kanneganti, T. D. Caspase-6 is a key regulator of innate immunity, inflammasome activation, and host defense. *Cell* **181**, 674 (2020).
17. Wan, H. et al. Voltage-dependent anion channel 1 oligomerization regulates PANoptosis in retinal ischemia–reperfusion injury. *Neural Regen Res.* **21**, 1652 (2026).
18. Heo, J. et al. Machine learning–based model for prediction of outcomes in acute stroke. *Stroke* **50**, 1263–1265 (2019).
19. Reel, P. S., Reel, S., Pearson, E., Trucco, E. & Jefferson, E. Using machine learning approaches for multi-omics data analysis: a review. *Biotechnol. Adv.* **49**, 107739 (2021).
20. Su, J. et al. Identification of Endoplasmic reticulum stress-related biomarkers of diabetes nephropathy based on bioinformatics and machine learning. *Front. Endocrinol.* **14**, 1206154 (2023).
21. Longa, E. Z., Weinstein, P. R., Carlson, S. & Cummins, R. Reversible middle cerebral artery occlusion without craniectomy in rats. *Stroke* **20**, 84–91 (1989).
22. Bieber, M. et al. Validity and reliability of neurological scores in mice exposed to middle cerebral artery occlusion. *Stroke* **50**, 2875–2882 (2019).
23. Chen, J. et al. Therapeutic benefit of intravenous administration of bone marrow stromal cells after cerebral ischemia in rats. *Stroke* **32**, 1005–1011 (2001).
24. Desland, F. A., Afzal, A., Warraich, Z. & Mocco, J. Manual versus automated rodent behavioral assessment: comparing efficacy and ease of Bederson and Garcia neurological deficit scores to an open field video-tracking system. *J. Cent. Nerv. Syst. Dis.* **6**, 7 (2014).
25. Stamova, B. et al. Gene expression in peripheral immune cells following cardioembolic stroke is sexually dimorphic. *PLOS One.* **9**, e102550 (2014).
26. Barr, T. L. et al. Genomic biomarkers and cellular pathways of ischemic stroke by RNA gene expression profiling. *Neurology* **75**, 1009 (2010).
27. Davis, S. & Meltzer, P. S. GEOquery: a Bridge between the gene expression omnibus (GEO) and bioconductor. *Bioinformatics* **23**, 1846–1847 (2007).
28. Song, F. et al. PANoptosis-based molecular subtyping and HPAN-index predicts therapeutic response and survival in hepatocellular carcinoma. *Front. Immunol.* **14**, 1197152 (2023).
29. Zheng, K. et al. Single-cell RNA-seq reveals the transcriptional landscape in ischemic stroke. *J. Cereb. Blood Flow. Metab.* **42**, 56 (2021).
30. Ritchie, M. E. et al. Limma powers differential expression analyses for RNA-sequencing and microarray studies. *Nucleic Acids Res.* **43**, e47 (2015).
31. Zhou, Y. et al. Metascape provides a biologist-oriented resource for the analysis of systems-level datasets. *Nat. Commun.* **10**, 1523 (2019).
32. Sánchez-Medina, A. J. & Galván-Sánchez, I. Fernández-Monroy, M. Applying artificial intelligence to explore sexual cyberbullying behaviour. *Heliyon* **6**, e03218 (2020).
33. Shi, H., Yuan, X., Liu, G. & Fan, W. Identifying and validating GSTM5 as an Immunogenic gene in diabetic foot ulcer using bioinformatics and machine learning. *J. Inflamm. Res.* **16**, 6241 (2023).
34. Wilkerson, M. D. & Hayes, D. N. ConsensusClusterPlus: a class discovery tool with confidence assessments and item tracking. *Bioinformatics* **26**, 1572 (2010).
35. Yu, G., Wang, L. G., Han, Y. & He, Q. Y. ClusterProfiler: an R package for comparing biological themes among gene clusters. *OMICS J. Integr. Biol.* **16**, 284 (2012).
36. Pereira, W. J. et al. Asc-seurat: analytical single-cell seurat-based web application. *BMC Bioinform.* **22**, 556 (2021).
37. Qin, Y., Yan, G., Qiao, Y., Wang, D. & Tang, C. Identification of hub genes based on integrated analysis of single-cell and microarray transcriptome in patients with pulmonary arterial hypertension. *BMC Genom.* **24**, 788 (2023).
38. Zhou, G. et al. NetworkAnalyst 3.0: a visual analytics platform for comprehensive gene expression profiling and meta-analysis. *Nucleic Acids Res.* **47**, W234 (2019).
39. Lyu, Z. et al. Destructive effects of pyroptosis on homeostasis of neuron survival associated with the dysfunctional BBB-glymphatic system and amyloid-beta accumulation after cerebral ischemia/reperfusion in rats. *Neural Plast.* **2021**, 4504363 (2021).
40. Tang, B., Li, Y., Xu, X., Du, G. & Wang, H. Electroacupuncture ameliorates neuronal injury by NLRP3/ASC/caspase-1 mediated pyroptosis in cerebral ischemia-reperfusion. *Mol. Neurobiol.* **61**, 2357–2366 (2024).
41. Ye, X. et al. Caspase-1: a promising target for preserving blood–brain barrier integrity in acute stroke. *Front. Mol. Neurosci.* **15**, 856372 (2022).
42. Makoni, N. J. & Nichols, M. R. The intricate biophysical puzzle of caspase-1 activation. *Arch. Biochem. Biophys.* **699**, 108753 (2021).
43. Ebstein, F. et al. PSMC3 proteasome subunit variants are associated with neurodevelopmental delay and type I interferon production. *Sci. Transl Med.* **15**, eabo3189 (2023).
44. Liu, Y. et al. PSMD2 contributes to the progression of esophageal squamous cell carcinoma by repressing autophagy. *Cell. Biosci.* **13**, 67 (2023).
45. Wang, S., Wang, H., Zhu, S. & Wang, Z. PSMD2 promotes the progression of bladder cancer and is correlated with immune infiltration. *Front. Oncol.* **12**, 1058506 (2022).
46. Zhao, H. & Lu, G. Prognostic implication and immunological role of PSMD2 in lung adenocarcinoma. *Front. Genet.* **13**, 905581 (2022).
47. Chen, K. Y., Huang, L. M., Kung, H. J., Ann, D. K. & Shih, H. M. The role of tyrosine kinase etk/bmx in EGF-induced apoptosis of MDA-MB-468 breast cancer cells. *Oncogene* **23**, 1854–1862 (2004).
48. Wu, J. C. C. et al. Location and level of Etk expression in neurons are associated with varied severity of traumatic brain injury. *PLOS One.* **7**, e39226 (2012).
49. Eißmann, M. et al. Overexpression of the anti-apoptotic protein AVEN contributes to increased malignancy in hematopoietic neoplasms. *Oncogene* **32**, 2586–2591 (2013).
50. Luo, Q. et al. Targetable leukaemia dependency on noncanonical PI3Kγ signalling. *Nature* **630**, 198–205 (2024).

51. Lin, Y. C., Lu, Y. H., Lee, Y. C., Hung, C. S. & Lin, J. C. Altered expressions and splicing profiles of *Acin1* transcripts differentially modulate brown adipogenesis through an alternative splicing mechanism. *Biochim. Biophys. Acta BBA - Gene Regul. Mech.* **1863**, 194601 (2020).
52. Fan, D., Cong, Y., Liu, J., Zhang, H. & Du, Z. Spatiotemporal analysis of mRNA-protein relationships enhances transcriptome-based developmental inference. *Cell. Rep.* **43**, 113928 (2024).
53. Slavov, N. Unpicking the proteome in single cells. *Science* **367**, 512–513 (2020).
54. D'Antona, S., Porro, D., Gallivanone, F. & Bertoli, G. Characterization of cell cycle, inflammation, and oxidative stress signaling role in non-communicable diseases: insights into genetic variants, MicroRNAs and pathways. *Comput. Biol. Med.* **174**, 108346 (2024).
55. Samareh, A. et al. Diagnostic potential of NEAT1, hsa-let-7a-5p, and miR-506-3p in early-stage parkinson's disease. *Curr. Med. Chem.* **32**, 1–15 .
56. Ueta, M. et al. Positive regulation of innate immune response by miRNA-let-7a-5p. *Front. Genet.* **13**, 1025539 (2023).
57. Zhou, B. et al. Hsa-let-7c-5p augments enterovirus 71 replication through viral subversion of cell signaling in rhabdomyosarcoma cells. *Cell. Biosci.* **7**, 7 (2017).
58. Gecys, D. et al. Circulating hsa-let-7e-5p and hsa-miR-125a-5p as possible biomarkers in the diagnosis of major depression and bipolar disorders. *Dis. Markers* **2022**, 3004338 (2022).
59. Sugiura, S. et al. CRE-mediated gene transcription in the peri-infarct area after focal cerebral ischemia in mice. *J. Neurosci. Res.* **75**, 401–407 (2004).
60. Mabuchi, T. et al. Phosphorylation of cAMP response element-binding protein in hippocampal neurons as a protective response after exposure to glutamate in vitro and ischemia in vivo. *J. Neurosci.* **21**, 9204 (2001).
61. Nakajima, T. et al. Relationship between the activation of Cyclic AMP responsive element binding protein and ischemic tolerance in the penumbra region of rat cerebral cortex. *Neurosci. Lett.* **331**, 13–16 (2002).
62. Tanaka, K. et al. Temporal profile of CREB phosphorylation after focal ischemia in rat brain. *Neuroreport* **10**, 2245 (1999).
63. Gu, X. et al. Fisetin alleviates cerebral ischemia/reperfusion injury by regulating Sirt1/Foxc1/Ubqln1 pathway-mediated proteostasis. *Int. Immunopharmacol.* **130**, 111742 (2024).
64. Allen, C. et al. Neutrophil cerebrovascular transmigration triggers rapid neurotoxicity through release of proteases associated with de-condensed DNA. *J. Immunol. Baltim. Md.* **1950 189**, 381 (2012).
65. Stowe, A. M. et al. Neutrophil elastase and neurovascular injury following focal stroke and reperfusion. *Neurobiol. Dis.* **35**, 82 (2009).
66. Strbian, D., Karjalainen-Lindsberg, M. L., Tatlisumak, T. & Lindsberg, P. J. Cerebral mast cells regulate early ischemic brain swelling and neutrophil accumulation. *J. Cereb. Blood Flow. Metab.* **26**, 605–612 (2006).
67. Greco, R. et al. Characterization of CB2 receptor expression in peripheral blood monocytes of acute ischemic stroke patients. *Transl Stroke Res.* **12**, 550–558 (2021).
68. Boyette, L. B. et al. Phenotype, function, and differentiation potential of human monocyte subsets. *PLOS One.* **12**, e0176460 (2017).
69. Gan, Y. et al. Ischemic neurons recruit natural killer cells that accelerate brain infarction. *Proc. Natl. Acad. Sci. U S A.* **111**, 2704 (2014).
70. Endres, M. et al. Immune pathways in etiology, acute phase, and chronic sequelae of ischemic stroke. *Circ. Res.* https://doi.org/10.1161/CIRCRESAHA.121.319994 (2022).
71. Selvaraj, U. M. et al. Delayed egress of CD8 T cells contributes to long-term pathology after ischemic stroke in male mice. *Brain Behav. Immun.* **95**, 502 (2021).
72. Liesz, A., Hu, X., Kleinschnitz, C. & Offner, H. The functional role of regulatory lymphocytes in stroke: facts and controversies. *Stroke J. Cereb. Circ.* **46**, 1422 (2015).
73. Sakaguchi, S. & Regulatory, T. Cells: key controllers of Immunologic self-tolerance. *Cell* **101**, 455–458 (2000).
74. Gee, J. M., Kalil, A., Thullbery, M. & Becker, K. J. Induction of Immunologic tolerance to Myelin basic protein prevents central nervous system autoimmunity and improves outcome after stroke. *Stroke J. Cereb. Circ.* **39**, 1575 (2008).
75. Shapouri-Moghaddam, A. et al. Macrophage plasticity, polarization, and function in health and disease. *J. Cell. Physiol.* **233**, 6425–6440 (2018).

Acknowledgements

We confirm that all methods were carried out in accordance with relevant guidelines and regulations. We thank all investigators contributed to this article.

Author contributions

X.C. and Q.Y. conceived and designed the study. X.C., Y.R., H.W., QH.Y., L.Z., Y.T., Y.W., J.W., Q.Y., J.W., and L.W. , contributed to the methodology. X.C., H.W., Y.R., and J.W. performed validation and wrote the original draft. X.C., Y.T., Y.W., QH.Y, HT, and Y.Z. curated the data. X.C., L.Z., H.W., and X.X. contributed to visualization. X.C. wrote, reviewed, and edited the manuscript. L.Z., Y.R., J.H., and Q.Y., supervised the study. Q.Y., Y.R., and J.H. acquired funding. All authors read and approved the final manuscript.

Funding

This study was supported by grants from the National Natural Science Foundation of China (Grant no. 82171456, 81971229) to Qin Yang; The First Affiliated Hospital of Chongqing Medical University, Doctoral Program of The First Affiliated Hospital of Chongqing Medical University (Grant no. CYYY-BSYJSKYCXXM202427) to Yu Ren; The Natural Science Foundation of Sichuan Provincial (Grant no. 2025ZNSFSC0589), and Health Commission of Sichuan Province Medical Science and Technology Program (Grant no. 24QNMP024 and 24WSXT075) to Jiagui Huang.

Declarations

Competing interests

The authors declare no competing interests.

Ethics approval

All animal experiments were approved by the Institutional Animal Care and Use Committee of Chongqing Medical University (approval code: IACUC-CQMU-2023-03015).

Additional information

Supplementary Information The online version contains supplementary material available at https://doi.org/10.1038/s41598-025-20997-5.

Correspondence and requests for materials should be addressed to J.H. or Q.Y.

Reprints and permissions information is available at www.nature.com/reprints.

Publisher's note Springer Nature remains neutral with regard to jurisdictional claims in published maps and institutional affiliations.